Magnetocaloric effects in rare-earth magnetic materials

A. S. Andreenko, K. P. Belov, S. A. Nikitin, and A. M. Tishin

M. V. Lomonosov State University, Moscow

Ups. Fiz. Nauk **158**, 553–579 (August 1989)

A review is given of the experimental investigations of the magnetocaloric effect (MCE) in rare-earth magnetic materials of different classes: heavy rare-earth metals and their alloys, iron garnets, and intermetallic compounds. The results of measurements of the MCE near phase transitions are given for the vicinity of the Curie and Néel temperatures, and also near magnetic compensation points in the case of ferromagnetism–helicoidal antiferromagnetism and helicoidal ferromagnetism–paramagnetism transitions. The contributions to the MCE made by the various magnetic sublattices in rare-earth ferromagnets are identified. Measurements of the MCE in single crystals of alloys of heavy rare-earth metals have made it possible to identify the main energy contributions to the helicoidal antiferromagnetism–ferromagnetism phase transitions and their energy dependences. The concluding section of the review deals with the technical applications of the MCE exhibited by rare-earth magnetic materials. An analysis is made of the potential applications as refrigerants in magnetic refrigerators, in thermodynamic cycles, and in structures of various types.

I. INTRODUCTION

A magnetic field acting on a substance alters its magnetic state and, consequently, it changes the internal magnetic energy, so that heat is evolved or absorbed reversibly. Under adiabatic conditions, for example when a magnetic field is switched on or off rapidly, the evolution or absorption of heat is manifested as an increase or a reduction in temperature. This is known as the magnetocaloric effect (MCE). We shall show that the MCE is due to a change in the entropy of the magnetic subsystem. The MCE is attracting the interest of both physicists and engineers: physicists because of potential applications in the study of interactions and changes in magnetic structures in magnetic materials, whereas engineers are hoping to be able to construct new devices and cooling systems.

In the case of magnetically ordered samples it is possible to distinguish the contributions to the MCE due to: 1) the paraprocess (i.e., the change in the exchange energy); 2) the rotation of the vector $\mathbf{I}_s$ (i.e., the change in the magnetic anisotropy energy). The first of them was discovered in 1918 by Weiss and Piccard[1] in nickel at a temperature close to the Curie point T_C, where in accordance with the thermodynamic equation

$$\Delta T = -\frac{T}{C_{P,H}}\left(\frac{\partial I}{\partial T}\right)_{P,H}\Delta H \qquad (1.1)$$

it can reach the highest values (in the case of Ni it is of the order of ~ 1 K in a field of 10^4 Oe), because the derivative $(\partial I/\partial T)_{P,H}$ has the highest value near T_C.

A second, finer effect, was first observed in 1939 by Kirenskiĭ.[2] He established that rapid rotation of a single-crystal nickel sphere in a magnetic field $H = H_s$, i.e., an adiabatic change of the direction of the vector $\mathbf{I}_s$ relative to the crystallographic axes changes the temperature of the sphere by about 10^{-3} K (at $T \approx 78$ K). In the case of a cubic single crystal this effect is described by[3]

$$\Delta T = \frac{T}{C_{P,H}}\left(\frac{\partial K_1}{\partial T}\right)_{P,H}\Delta\sum_{i\neq j} S_i^2 S_j^2, \qquad (1.2)$$

where K_1 is the magnetocrystalline anisotropy constant. It follows from the above equation that changes in the direction cosines S_i and S_j of the vector $\mathbf{I}_s$ in a crystal alter its temperature. This effect becomes perceptible at low temperatures when the derivative $(\partial K_1/\partial T)_{P,H}$ for Ni reaches high values.

Magnetically ordered materials exhibit not only the reversible MCE, but also magnetothermal effects which are accompanied by irreversible displacements of domain walls and irreversible rotation of the magnetization vector, and by magnetic relaxation phenomena (magnetic viscosity). These thermal effects are due to energy lost in the course of magnetization and they are sometimes called the irreversible MCE. In one cycle of variation of a magnetic field such effects make a very small contribution ΔT in the case of the majority of magnetically ordered substances.[40] Irreversible hysteretic effects appear in rare-earth metals and their alloys mainly in the region of the antiferromagnetism–ferromagnetism transition where a hysteresis loop widens. In low fields a hysteresis loop is very narrow so that the magnitude of the MCE, measured when the field is increased from 0 to H, becomes practically constant for rare-earth metals and their alloys when the cycles of application and removal of the field are repeated.

2. MAGNETOCALORIC EFFECTS IN RARE-EARTH FERRIMAGNETS (IRON GARNETS AND INTERMETALLIC COMPOUNDS)

In this section we shall consider the MCEs in rare-earth iron garnets and in intermetallic compounds during magnetization.

The behavior of the MCE in ferrimagnets differs considerably from that in ferromagnets. The temperature dependences of the MCE in a field of 16 kOe obtained[4,5] for polycrystalline Y and Gd iron garnets and for $Li_2O \cdot 2.5Fe_2O_5 \cdot 2.5Cr_2O_3$ ferrite spinel are compared in Fig. 1.

It is clear from Fig. 1 that the MCE in the case of yttrium iron garnet is positive throughout the investigated range of temperatures and near T_C it has a maximum typical of magnetically ordered substances. Cooling reduces the effect monotonically. The temperature dependence of the MCE can be calculated using Eq. (1.1) if we bear in mind that yttrium iron garnet behaves as an ordinary ferromagnet

 0038-5670/89/080649-16$01.80

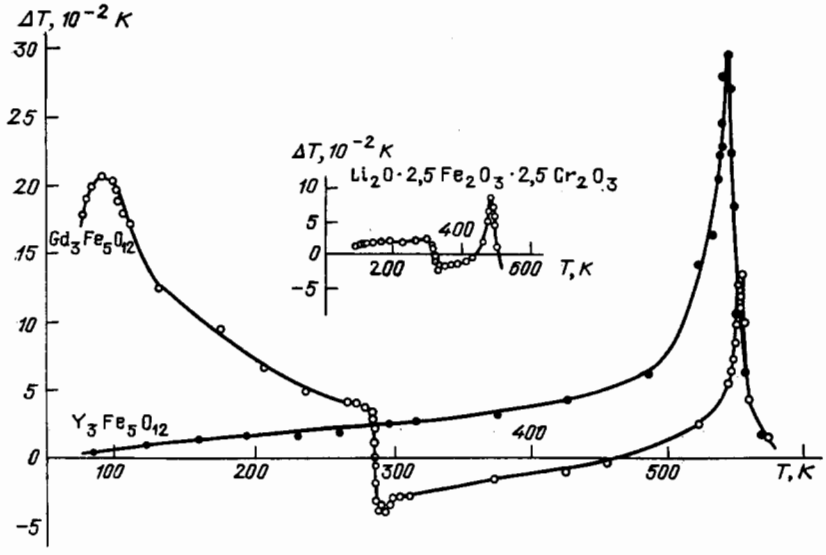

FIG. 1. Magnetocaloric effect in yttrium and gadolinium iron garnets, and in $Li_2 \cdot 2.5Fe_2O_3 \cdot 2.5Cr_2O_3$ in a magnetic field of 16 kOe.

[it exhibits the normal "Weiss" $I_s(T)$ curve, since both its iron sublattices a and d can be regarded as one "combined" sublattice]. As pointed out above, the MCE maximum at the Curie point appears because the derivative of the magnetization with respect to temperature reaches its maximum near T_C.

The MCE curve of gadolinium iron garnet (Fig. 1) is more complex. This is due to the influence of the gadolinium sublattice on the thermal state of the ferrite. This ferrite has a magnetic compensation point T_k near room temperature ($T_k = 285$ K). At this temperature the sign of the MCE is reversed from positive to negative and then, as a result of further heating between T_k and T_C, it becomes positive again when the effect reaches its maximum at T_C.[1)] This effect is explained in Ref. 7 and discussed in greater detail by the molecular field method in Refs. 8 and 9. Reversal of the sign of the MCE at the compensation point T_k is due to the magnetic sublattice structure of ferrites; each of the magnetic sublattices makes its own characteristic contribution to the resultant MCE of the ferrite. The difference between the contributions made by the sublattices to the MCE is manifested particularly clearly in the case of rare-earth iron garnets. We shall consider this point in the specific case of gadolinium iron garnet. The amount of heat released as a result of the MCE is an additive sum of the amounts of heat released in the sublattice of the iron ions ΔQ_{Fe} and in the sublattice of the gadolinium ions ΔQ_{Gd}:

$$\Delta Q = \Delta Q_{Fe} + \Delta Q_{Gd}.$$

The amount of heat released in the iron sublattice is

$$\Delta Q_{Fe} = -T\left(\frac{\partial \mathbf{I}_{Fe}}{\partial T}\right)_{P,H} \Delta \mathbf{H}. \qquad (2.1)$$

The amount of heat released in the gadolinium sublattice is

$$\Delta Q_{Gd} = -T\left(\frac{\partial \mathbf{I}_{Gd}}{\partial T}\right)_{P,H} \Delta \mathbf{H}, \qquad (2.2)$$

where $\mathbf{I}_{Fe}$ and $\mathbf{I}_{Gd}$ are the magnetizations of the iron and gadolinium sublattices. (In these relationships $\mathbf{I}_{Fe}$, $\mathbf{I}_{Gd}$, and $\mathbf{H}$ are vector quantities.) It follows from neutron diffraction data[16,55-57] that the magnetizations $\mathbf{I}_{Fe}$ and $\mathbf{I}_{Gd}$ are directed opposite to one another and that at temperatures $T < T_k$ we have $I_{Gd} > I_{Fe}$, whereas at $T > T_k$, we find that $I_{Gd} < I_{Fe}$. Application of a magnetic field at temperatures below T_k produces a positive effect ΔQ_{Gd}, since the vector $\mathbf{I}_{Gd}$, coincides with the direction of $\mathbf{H}$, whereas ΔQ_{Fe} is negative since the vector $\mathbf{I}_{Fe}$ is directed against $\mathbf{H}$. Conversely, above T_k the value of ΔQ_{Gd} is negative and that of ΔQ_{Fe} is positive.

The physical reason for the reversal of the sign of the MCE due to the transition at T_k is that the paraprocess observed in the Gd sublattice at $T < T_k$ is of the "ferromagnetic" type (when the field $\mathbf{H}$ reduces the magnetic entropy S_M), whereas in the range $T > T_k$ where the vectors $\mathbf{I}_{Gd}$ and $\mathbf{H}$ are antiparallel, the paraprocess is of the "antiferromagnetic" type[7,10,11] (when the field $\mathbf{H}$ increases S_M). Conversely, in the Fe sublattice when $T < T_k$ we observed the "antiferromagnetic" paraprocess, whereas at temperatures $T > T_k$ the paraprocess is "ferromagnetic." However, the paraprocess in the Gd sublattice is stronger than that in the Fe sublattice, so that the behavior of the MCE in the vicinity of T_k is governed almost entirely by the Gd sublattice.

We shall now consider in greater detail the behavior of the MCE in the range $T < T_k$. Figure 2(a) shows schematically the temperature dependences of the magnetizations of the gadolinium sublattice (curve C) and the "resultant"

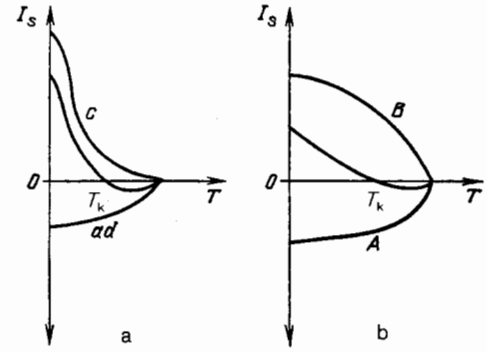

FIG. 2. Schematic form of the temperature dependences of the sublattice magnetizations plotted for gadolinium iron garnet (a) and lithium ferrite spinel (b).

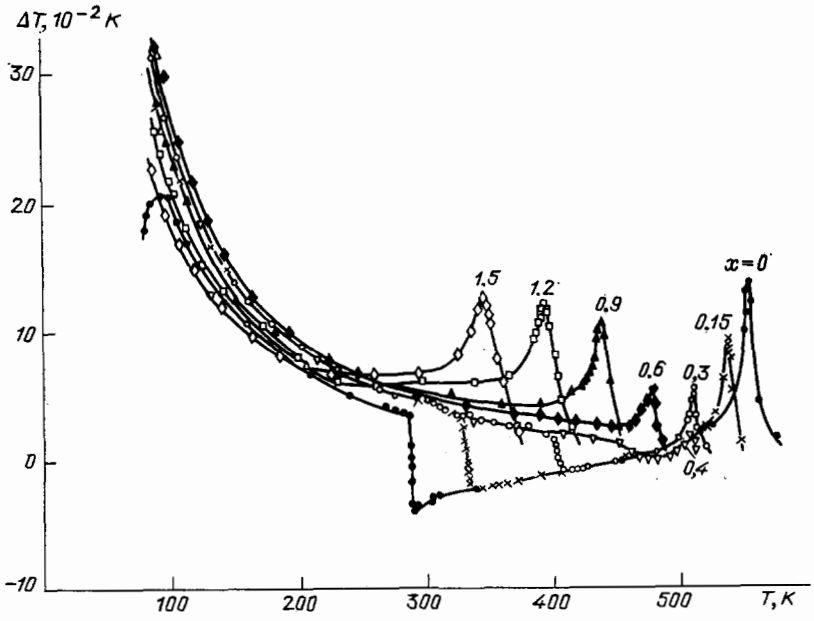

FIG. 3. Temperature dependences of the magnetocaloric effect obtained for substituted $Gd_3Ga_xFe_{5-x}O_{12}$ ($x = 0 - 1.5$) iron garnets in a field $H = 16$ kOe.

iron sublattice (curve *ad*).[10] According to Ref. 10, the $I_{Gd}(T)$ curve is strongly broadened because the Gd^{3+} ions are affected by a weaker exchange field (mainly the exchange field of the iron sublattice) than the field acting between iron ions. It follows that at low temperatures the subsystem of the Gd^{3+} ions is largely in a disordered state and that a strong paraprocess is expected on application of an external field so that, consequently, the MCE should be strong, since the derivative $\partial I_{Gd}/\partial T$ is large [see Eq. (2.2)]. In other words, a major change in the magnetic anisotropy, ΔS_M, occurs in the gadolinium sublattice at low temperatures when the magnetic field is applied.

Since in the adiabatic process the sum of the magnetic entropy S_m and of the crystal lattice entropy S_{latt} is constant:

$$S_M + S_{latt} = \text{const}, \tag{2.3}$$

it follows that S_{latt} increases, i.e., a strong positive MCE appears in the gadolinium sublattice. Consequently, the "resultant" iron sublattice has an $I_{Fe}(T)$ curve of the Weiss type [curve *ad* in Fig. 2(a)]. Below the Curie point the temperature dependence of S_M is slight and, consequently, the released heat ΔQ_{Fe} is also small, since the derivative $\partial I_{Fe}/\partial T$ is considerably less than $\partial I_{Gd}/\partial T$ [see Eqs. (2.1) and (2.2)]. It therefore follows that the net MCE observed in Gd iron garnet at low temperatures (and in the vicinity of T_k) is governed almost completely by the component ΔQ_{Gd}.

One further feature illustrated in Fig. 1 should be mentioned: at 90 K the MCE has its maximum. This maximum occurs at what is called a low-temperature point T_{lt} at which there is an abrupt change in the magnetic order in the Gd sublattice. The existence of this point was predicted and confirmed experimentally in Refs. 9–11.

The inset in Fig. 1 gives the results of measurements[4] of the MCE in lithium ferrite spinel which has a magnetic compensation point T_k. We can see that there is again a reversal of the sign of the MCE at T_k. However, the low-temperature MCE of this compound is slight and, in contrast to gadolinium iron garnet, it has a tendency to decrease as a result of cooling. This is due to the fact that the magnetic ions in both sublattices (A and B) in this ferrite experience strong exchange fields and, consequently, they both exhibit Weiss curves $I_A(T)$ and $I_B(T)$ (Fig. 2b), whereas the application of a field H induces a weak paraprocess and, consequently, the values of ΔQ_A and ΔQ_B are small.

Replacement of the Fe^{3+} ions in gadolinium iron garnet with nonmagnetic ions can reduce the exchange field acting on the Gd^{3+} ions even further and thus create conditions favorable for a strong low-temperature paraprocess and, consequently, for high values of the MCE in the gadolinium sublattice. Figure 3 shows the MCE curves for the $Gd_3Ga_xFe_{5-x}O_{12}$ system with $0 \leqslant x \leqslant 1.5$ (Ref. 12). We can see that at low temperatures the MCE is 2–3 times greater than at the Curie points. In the limiting case of complete replacement of Fe^{3+} with Ga^{3+} the result is antiferromagnetic garnet gallate $Gd_3Ga_5O_{12}$. Figure 4 gives the MCE curves based on the results of Ref. 63. We can see that in the vicinity of the Néel point the effect reaches an unusually high value, which is the result of a major change in the magnetic energy entropy S_M in fields of 30–40 kOe.

Figure 5 gives the temperature dependences of the MCE obtained in a field of 16 kOe for iron garnets of heavy rare-earth elements.[13] In the case of Tb, Dy, Ho, and Er iron garnets the $\Delta T(T)$ curves are similar to the corresponding curve of $Gd_3Fe_5O_{12}$ (the sign of ΔT is reversed in the vicinity

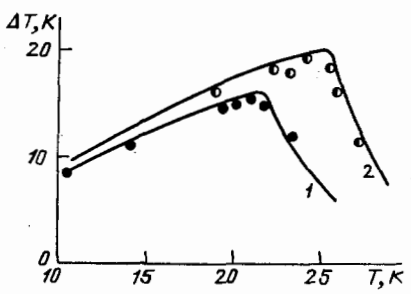

FIG. 4. Magnetocaloric effect in $Gd_3Ga_5O_{12}$ subjected to fields $H = 32.6$ kOe (1) and 46.5 kOe (2).

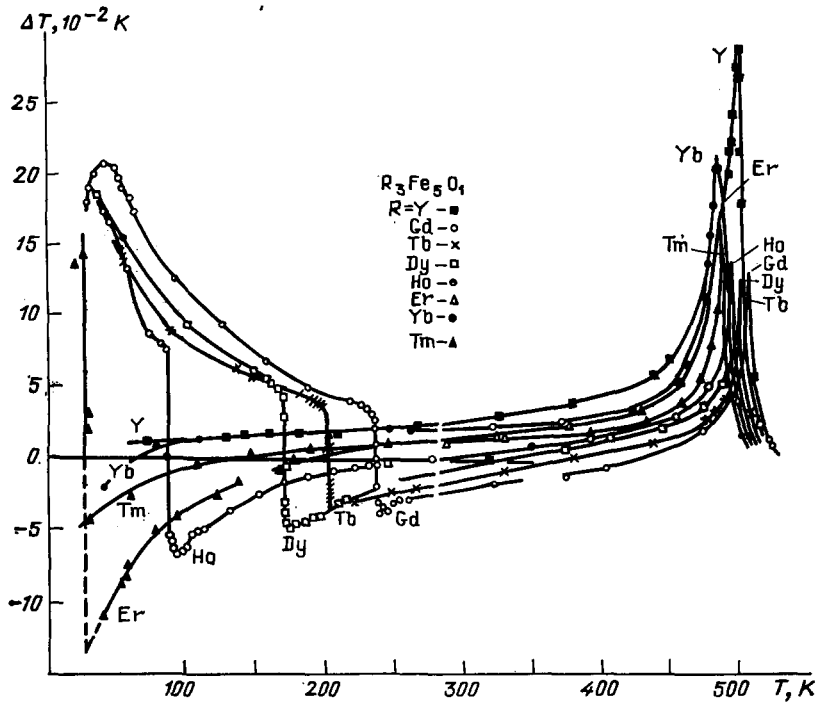

FIG. 5. Temperature dependences of the magnetocaloric effect in Y, Gd, Tb, Dy, Ho, Er, Yb, and Tm iron garnets in a field $H = 16$ kOe.

of the compensation points T_k and there is a strong increase of the positive ΔT in the region below T_k). The low-temperature points T_{lt} of these materials lie at higher temperatures.

The magnetic compensation temperatures of Tm and Yb iron garnets are located at helium temperatures and the characteristic features of the behavior of the MCE in such iron garnets has not yet been investigated. It follows from Ref. 14, reporting measurements of the MCE in these ferrites subjected to fields up to 110 kOe, that the effect is negative at helium temperatures. In the region of T_k the MCE may also include a contribution of a small irreversible thermal effect[19] associated with the first-order magnetic phase transition in the field at temperatures close to T_k.

The results of measurements of the MCE in gadolinium iron garnet were used in Ref. 15 to find H_{eff2}, which is the effective field exerted by the iron sublattice on the Gd^{3+} ions. According to Ref. 16, this field can be deduced from the relationship

$$(\Delta T)_{Gd} = \frac{2S_2}{g_J J_2 C_P} H_{eff2}\chi_m H, \qquad (2.4)$$

where S_2 is the spin of the Gd^{3+} ion; $J_2 = S_2$; χ_m is the molar susceptibility of the Gd sublattice; C_P is the specific heat. Application of Eq. (2.4) to $Gd_3Fe_5O_{12}$ yields the value $H_{eff2} = 258$ kOe, whereas the corresponding field for $Gd_3Ga_{0.3}Fe_{4.7}O_{12}$ is $H_{eff2} = 232$ kOe, which agrees with the values of H_{eff2} deduced from the magnetic data.

Investigations of the MCE in intermetallic compounds $TbFe_2$, $ErFe_2$, $HoFe_3$, and also in YFe_2 and YFe_3 were reported in Refs. 17 and 18. Figure 6 gives the temperature dependence of the MCE in $ErFe_2$, $HoFe_2$, YFe_3, and YFe_2 ($H = 15.8$ kOe). Both YFe_2 and YFe_3 behave as ordinary ferromagnets in respect of the MCE, because yttrium has no

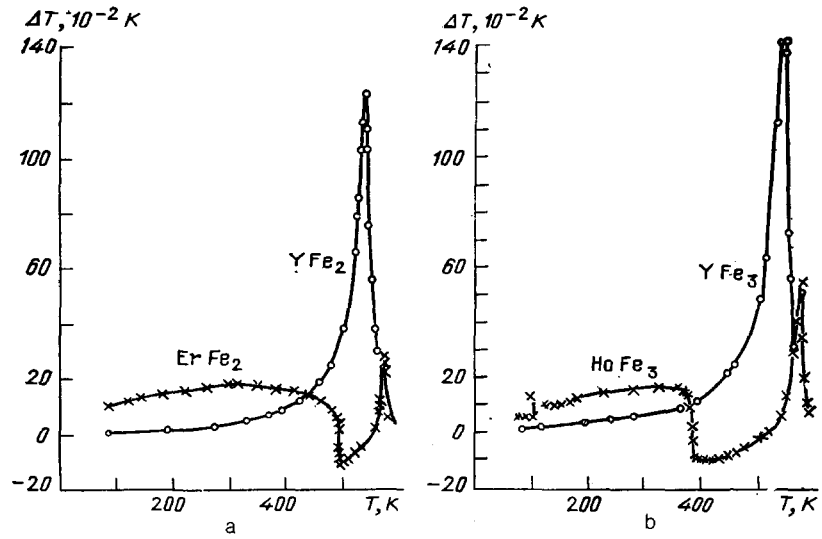

FIG. 6. Temperature dependences of the magnetocaloric effect for compounds YFe_2, $ErFe_2$ (a) and YFe_3, $HoFe_3$ (b) in a field of 15.8 kOe.

TABLE I. Curie temperatures T_C and magnetic compensation temperatures T_k of rare-earth compounds found by measuring the magnetocaloric effect and the magnitude of this effect at $T = T_C$.

Compound	T_C, K	T_k, K	ΔT, K, at $T=T_C$
$Gd_3Ga_xFe_{5-x}O_{12}$			
$x = 0.3$	511	402	0,05 [12], 16 kOe
$x = 0.4$	507	472	0,02 [12], 16 kOe
$x = 0.9$	438	—	0,11 [12], 16 kOe
$x = 1.5$	344	—	0,13 [12], 16 kOe
$x = 5.0$	—	—	20,5 [63], 46,5 kOe
$R_3Fe_5O_{12}$			
R = Y	545	—	0,28 [13], 16 kOe
R = Gd	556	286	0,14 [13], 16 kOe
R = Tb	548	250	0,12 [13], 16 kOe
R = Dy	547	220	0,13 [13], 16 kOe
R = Ho	535	140	0,14 [13], 16 kOe
R = Er	535	80	0,18 [13], 16 kOe
R = Yb	530	5	0,22 [13, 19], 16 kOe
R = Tm	536	5	0,15 [13, 19], 16 kOe
$TbFe_2$	695	—	0,7 [17, 18], 15,8 kOe
$ErFe_2$	575	490	0,3 [17, 18], 15,8 kOe
$HoFe_3$	574	389	0,57 [17, 18], 15,8 kOe
YFe_2	535	—	1,25 [17, 18], 15,8 kOe
YFe_3	535	—	1,43 [17, 18], 15,8 kOe
$Dy_3Al_5O_{12}$	$T_N = 2.54$	—	18 [63], 20 kOe

magnetic moment, and they only have a maximum of ΔT at the Curie point. The compounds $ErFe_2$ and $HoFe_3$ are two-sublattice ferrimagnets exhibiting the compensation points located above room temperature. The MCE near T_k behaves in these compounds similarly to the effect observed in gadolinium iron garnet: heating of a sample reverses the sign of the MCE from positive to negative at $T = T_k$. Since a strong exchange field ($H_{eff} \sim 10^6$ Oe) acts in the rare-earth sublattices of these compounds,[18,19] the change in the magnetic anisotropy in the applied field at temperatures $T < T_k$ is less for these compounds than for rare-earth iron garnets. The MCE in these compounds behaves approximately in the same way as in the case of lithium ferrite spinel.

We shall conclude this section by noting that measurements of the MCE are used widely in laboratory practice to find the temperatures of magnetic phase transitions at which this effect reaches its maximum or shows reversal of sign. Table I gives the Curie temperatures T_C, the magnetic compensation points T_k, and the value of the MCE at $T = T_C$ of rare-earth magnetic materials.

3. MAGNETOCALORIC EFFECTS IN RARE-EARTH METALS AND THEIR ALLOYS

When the MCE is measured in rare-earth metals and alloys it is very important to ensure that the magnetic field is sufficiently high so as to exceed the effective magnetic anisotropy fields and the critical magnetic fields which destroy antiferromagnetic helical structures existing in a majority of these metals and their alloys. This makes it necessary to use superconducting solenoids where magnetic fields 50–80 kOe can be created.

The MCE is usually measured by a method proposed by Weiss and his colleagues.[1] A sample is placed between the poles of an electromagnet and rapid switching on or off of the electromagnet ensures that measurements of the temperature of a sample are made under adiabatic conditions. This method was used by us to measure the MCE in fields up to 16 kOe. However, it is unsuitable for measurements in strong magnetic fields ($H > 16$ kOe) created by a superconducting solenoid. The time necessary to establish such a field with the aid of an electromagnet amounts to just a few seconds. However, when a magnetic field is created by a superconducting solenoid, it may take several minutes to establish a steady-state value. During this time interval a considerable amount of heat is dissipated as a result of the MCE in the investigated sample. Therefore, measurements of the MCE in strong magnetic fields should be carried out as follows.[65] Before beginning the measurements a sample is placed in a region where there is no magnetic field. Then, when a field of the required value is established in a solenoid, a sample is introduced into the solenoid at the highest possible velocity. The temperature of the sample is measured at the moment when it reaches the center of the solenoid. The MCE was studied using either cylinders 5–6 mm in diameter and 10–12 mm long, or disks ~5 mm in diameter and about 3 mm thick. Temperature measurements were made using a copper–iron–copper thermocouple. The temperature stabilization scheme employed for this purpose made it possible to maintain the temperature of a sample within 1×10^{-1} K. The MCE was measured in magnetic fields up to 60 kOe at temperatures 20–300 K. An analysis of the experimental errors showed that they amounted to 8–15% in the case of the MCE (depending on its magnitude).

Magnetic structures, the values of the maximum critical field for the destruction of the helicoidal antiferromagnetic ordering $(H_{cr})_{max}$, and the magnitude of the MCE at the magnetic ordering temperature are listed in Table II for heavy rare-earth metals and some of their alloys discussed in the present section.

Figure 7 gives the MCE curves of polycrystalline Gd in fields up to 70 kOe (Refs. 16, 41, and 64). In the region of T_C the value of ΔT is considerably greater than the corresponding effect in Ni. In the temperature range 200–230 K this metal exhibits a spin reorientation transition which is a second-order phase transition. However, it is accompanied by just a small change in the magnitude of the MCE.

TABLE II. Magnetic structures of heavy rare-earth metals and their alloys (FM denotes collinear ferromagnetism, HFM is helicoidal ferromagnetism, and HAFM is helicoidal antiferromagnetism), the maximum critical field for destruction of the antiferromagnetic order $(H_{cr})_{max}$, and the magnitude of the magnetocaloric effect at the temperature $\Theta_2(T_C)$ in a field directed along the easy magnetization axis.

Metal	Magnetic structure			$(H_{cr})_{max}$, Oe	ΔT_{max}, K
Gd	Fm, $T<T_C=293$ K			—	14 K [41], $H=70$ kOe
Tb	Fm, $T<\Theta_1=219$ K	HAFM, $\Theta_1<T<\Theta_2=230$ K		200	10,5 K [20], $H=60$ kOe
Dy	Fm, $T<\Theta_1=85$ K	HAFM, $\Theta_1<T<\Theta_2=178$ K		11 000	8,3 K [20], $H=60$ kOe
Ho	HFM, $T<\Theta_1=20$ K	HAFM, $\Theta_1<T<\Theta_2=133$ K		18 000	4,5 K [20], $H=60$ kOe
Er	HFM, $T<\Theta_1=20$ K	cycloidal structure $\Theta_1<T<\Theta_1^1=53$ K	sinusoidal structure $\Theta_1<T<\Theta_2=85$ K	18 000	3,2 K [20], $H=60$ kOe
Tm	Fm, $T<\Theta_1=25$ K	sinusoidal structure $\Theta_1<T<\Theta_2=60$ K		29 000	1,5 K [20], $H=60$ kOe
Alloys $Tb_{1-x}Gd_x$:					
$x=0.06$	Fm, $T<T_C=232$ K			—	—
$x=0.30$	Fm, $T<T_C=252$ K			—	3,0 K [62], $H=8$ kOe
$x=0.50$	Fm, $T<T_C=263$ K			—	—
$x=0.60$	Fm, $T<T_C=270$ K			—	—
$x=0.80$	Fm, $T<T_C=281$ K			—	2,3 K [62], $H=8$ kOe
$x=0.90$	Fm, $T<T_C=285$ K			—	—
$Tb_{0,835}Y_{0,165}$	Fm, $T<\Theta_1=120$ K	HAFM $\Theta_1<T<\Theta_2=205$ K		5 000	2,5 K [62], $H=8$ kOe

Figure 8 shows the experimentally determined[20] MCE curves of polycrystalline metals: Tb, Dy, Ho, Er, and Tm. The MCE was measured in the field of a superconducting solenoid ($H=60.2$ kOe). Clearly, the $\Delta T(T)$ curves obtained for Dy, Ho, Er, and Tm were very complex. In the interpretation of these curves we must bear in mind that variation of temperature of Tb, Dy, Ho, Er, and Tm metals induces the following magnetic phase transitions[16,19]: ferromagnetism–helicoidal antiferromagnetism (at $T=\Theta_1$) and helicoidal antiferromagnetism–paramagnetism (at $T=\Theta_2$). The former is a first-order transition and it is accompanied by an irreversible thermal effect (latent heat).

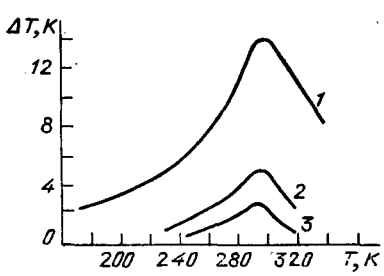

FIG. 7. Magnetocaloric effect in polycrystalline Gd subjected to the following fields H (kOe): (1) 70; (2) 20; (3) 10.

Figure 9(a) shows, by way of example, a schematic distribution of the magnetization vectors $\mathbf{I}_s$, relative to the hexagonal c axis of dysprosium. This scheme corresponds to a helicoidal antiferromagnetic structure, which—according to neutron diffraction data—exists in dysprosium in the absence of a magnetic field in the temperature range $\Theta_1-\Theta_2$ (85–178) K).[16,58] Within the limits of one basal plane the atomic magnetic moments become ferromagnetically ordered with the resultant magnetization I_s. In crossing over from one basal plane to another the vector $\mathbf{I}_s$ is rotated by a constant angle α. In an external field $H>H_{cr}$, directed along the easy magnetization axis (which is the a axis) this structure is destroyed and ferromagnetism is induced. The temperature $\Theta_1(H)$ shifts toward higher temperatures on increase in the field. Figure 9(b) shows schematically the changes in the $I_s(T)$ and $I(H)$ curves in the temperature range $\Theta_1-\Theta_2$. It should be pointed out that the temperature dependence of the critical field H_{cr} is complex [Fig. 9(b)]. The $I_s(T)$ and $I(H)$ curves are of abrupt nature since the transition at Θ_1 is of the first order, whereas the transition at Θ_2 (destruction of the magnetic order) is a second-order magnetic phase transition. In the case of Tb the tem-

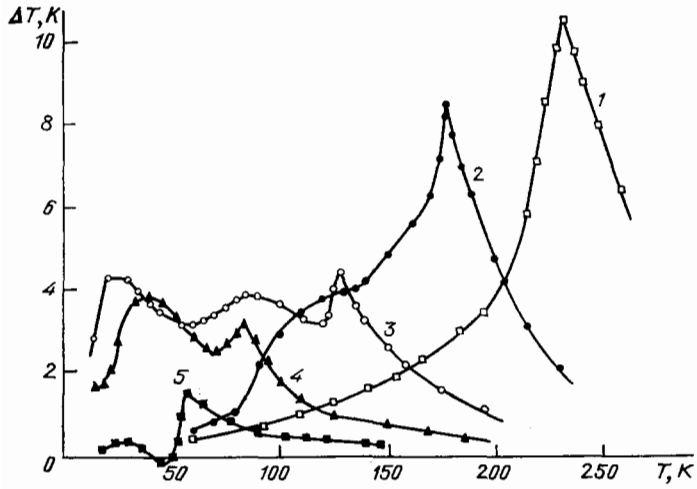

FIG. 8. Magnetocaloric effect in Tb (1), Dy (2), Ho (3), Er (4), and T (5) in a field $H = 60.2$ kOe.

perature Θ_1 (219 K) is located close to Θ_2 (230 K) and H_{cr} is very small (~ 200 Oe). Therefore, destruction of the helicoidal magnetic structure of this metal has almost no effect on the nature of the dependence $\Delta T(T)$ recorded in a field $H = 60.2$ Oe; the nature of this curve for Tb is the same as for Gd. In the case of Dy, Ho, Er, and Tm metals the $\Delta T(T)$ curves have not only maxima of ΔT corresponding to the transitions at $T = \Theta_2$, but also additional maxima which are associated with the transitions at $T = \Theta_1$. The critical fields for these metals are less than the applied field 60.2 kOe ($H_{cr} = 11$–29 kOe), as shown in Table II.

For example, in the case of Dy (Fig. 10) subjected to fields $H = 20.1$ and 30.2 kOe the temperature dependences of the MCE exhibit wide maxima in the interval 100–160 K because in fields $H > H_{cr}$ there is some heat evolved as a result of destruction of the helicoidal antiferromagnetic structure which exists in $H = 0$ at temperatures between $\Theta_1 = 85$ K and $\Theta_2 = 178$ K. At any temperature in the range $\Theta_1 - \Theta_2$ in fields $H > H_{cr}$ the MCE includes a contribution due to the absorption or evolution of heat as a result of the helicoidal antiferromagnetism–ferromagnetism transition. A further increase in the field flattens out this maximum because the paraprocess MCE increases with the field. In the region of the transition near H_{cr} there is an irreversible contribution to the MCE. In the case of Ho (curve 3 in Fig. 8) a maximum appears at $\Theta_1 = 20$ K ($\Delta T_{max} = 5.1$ K in a field $H = 60$ kOe) and at $\Theta_2 = 133$ K ($\Delta T_{max} = 4.5$ K in a field $H = 60$ kOe). The amplitude of the maximum at $T = \Theta_1$ is approximately the same as at $T = \Theta_2$. In the case of the $\Delta T(T)$ curve there is also a very small maximum at 70–90 K due to a complex temperature dependence of H_{cr}. In the range $\Theta_1 - \Theta_2$ the spin structure is helicoidal in the basal plane. The applied field destroys this structure and this contributes to the MCE. At temperatures $T < \Theta_1$, the MCE in Ho is due to deformation of the ferromagnetic helicoidal structure.

The temperature dependence of the MCE in Er (curve 4 in Fig. 8) has a maximum near $\Theta_2 = 85$ K. In a field $H = 60$ kOe the maximum MCE at 85 K is 3.2 K. Between $\Theta_1 = 20$ K and Θ_2, where in $H = 0$ there is a complex antiferromagnetic structure with an oscillatory component along the c axis, the $\Delta T(T)$ curve has a maximum due to suppression of this structure by the magnetic field. Like holmium, erbium exhibits a large MCE (about 3 K in a field $H = 60$ kOe) in a wide temperature range of 30–85 K.

The temperature dependence of the MCE of Tm (Fig. 11) has a maximum near the temperature $\Theta_2 = 60$ K. The value of ΔT is 1.5 K in a field $H = 60.2$ kOe. At lower tem-

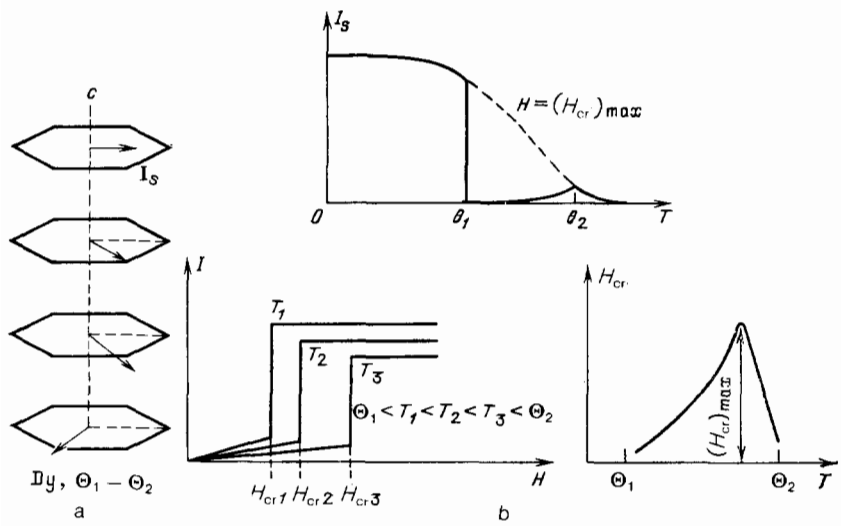

FIG. 9. (a) Schematic representation of the helicoidal antiferromagnetic structure of Dy in the range $\Theta_1 - \Theta_2$. (b) Schematic temperature dependences $I_S(T)$, $I(H)$, and $H_{cr}(T)$ for Dy.

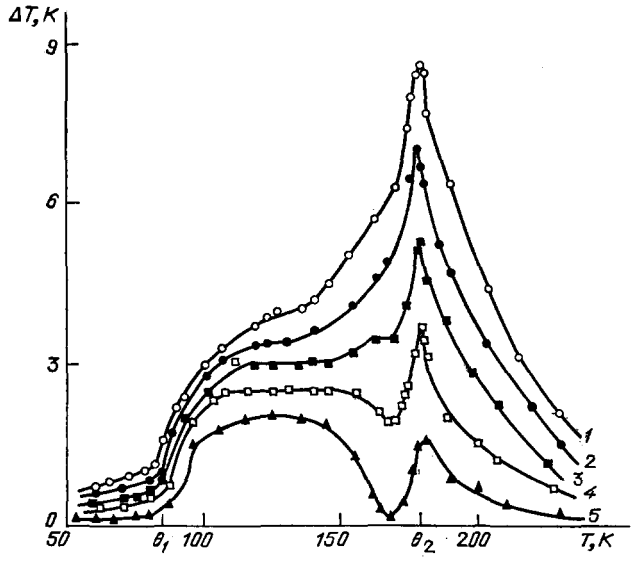

FIG. 10. Magnetocaloric effect in Dy recorded in different magnetic fields H (kOe): (1) 60.2; (2) 50.2; (3) 40.2; (4) 30.2; (5) 20.1.

peratures the ΔT effect becomes negative due to the absorption of heat on suppression of the antiferromagnetic structure by the applied magnetic field (according to the neutron diffraction data given in Ref. 21 this structure is in the form of a static longitudinal helical wave). At still lower tempertures the MCE becomes positive again and this is clearly due to the evolution of heat as a result of the interaction of the field with an antiphase ferrimagnetic structure which appears at temperatures below $\Theta_1 = 25$ K.

The experimental data obtained in Ref. 20 thus demonstrate that heavy rare-earth metals can exhibit a large MCE (up to 10 K in $H \sim 60$ kOe) in the vicinity of the magnetic phase transition points Θ_2 and Θ_1 (in the latter case this is due to the contribution made to the MCE by the heat of the antiferromagnetism–ferromagnetism transition).

It is interesting to consider the maximum values of the MCE which can be observed in this class of magnetic materials. Before finding this maximum, we must calculate the change in the magnetic part of the entropy $\Delta S_M (H,T)$ in an external magnetic field. In addition to the MCE data, we need to know the change in the specific heat of a rare-earth metal in a magnetic field: $C_P(H,T)$. There are no experimental data on the specific heat of rare-earth metals in strong magnetic fields. A closed cycle in an entropy diagram is used in Refs. 22 and 52 to obtain a thermodynamic relationship demonstrating that the influence of a magnetic field on the specific heat can be calculated if we know its value in the absence of a field $C_P(0,T)$ and the change in the temperature of a sample due to application of a field H:

$$C_P(H, T) = C_P(0, T - \Delta T)\frac{T}{T - \Delta T}\left(1 - \frac{d\Delta T}{dT}\right). \qquad (3.1)$$

It is clear from the above expression that the change in the specific heat in a field H is physically directly due to the magnetocaloric effect, i.e., it is governed by the change in the magnetic anisotropy in a field H.

A calculation of the influence of a field on the specific heat of heavy rare-earth metals, carried out in Ref. 23 using an expression identical with Eq. (3.1) above, shows that on application of a magnetic field the temperature dependence of the specific heat exhibits not only maxima at temperatures Θ_1 and Θ_2, but also additional features. In the case of dysprosium subjected to a field of $H = 20$ kOe there is an additional maximum at $T = \Theta_k = 160$ K (Fig. 12). Such anomalous behavior of the specific heat can be explained by the fact that in this range of temperatures the application of a field exceeding H_{cr} ($H > H_{cr}$) creates a fan magnetic structure in dysprosium. It is clear from Fig. 12 (curve 3) that an increase in the field destroys the singularities associated with the fan structure, which is in agreement with the magnetic data given in Ref. 24 on the transformation of the fan structure to the ferromagnetic order when the magnetic field is increased sufficiently. Reduction in the amplitudes of the specific heat peaks at temperatures Θ_1 and Θ_2 on increase in the magnetic field demonstrates suppression of spin fluctuations in a wide range of temperatures. An additional maximum in the range $H > H_{cr}$ exhibited by dysprosium at $T = \Theta_k \sim 165$ K demonstrates the existence of a tri-critical point where a line of first-order helicoidal antiferromagnetism–fan structure transitions goes over to a line of second-

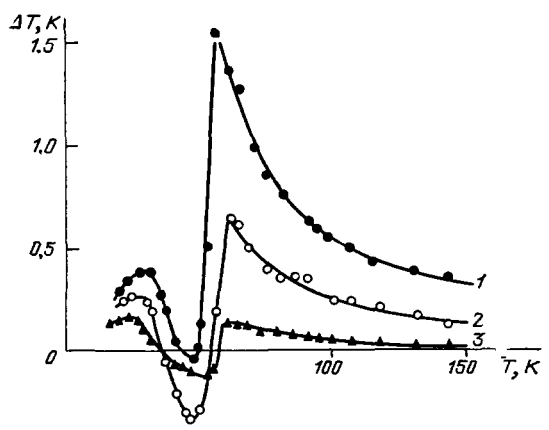

FIG. 11. Magnetocaloric effect in Tm in different magnetic fields H (kOe): (1) 60.2; (2) 40.2; (3) 20.1.

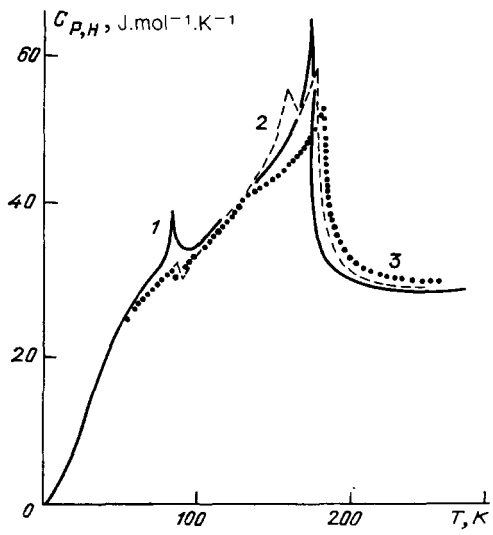

FIG. 12. Temperature dependences of the specific heat of Dy in different fields H (kOe): (1) 0; (2) 20; (3) 60.

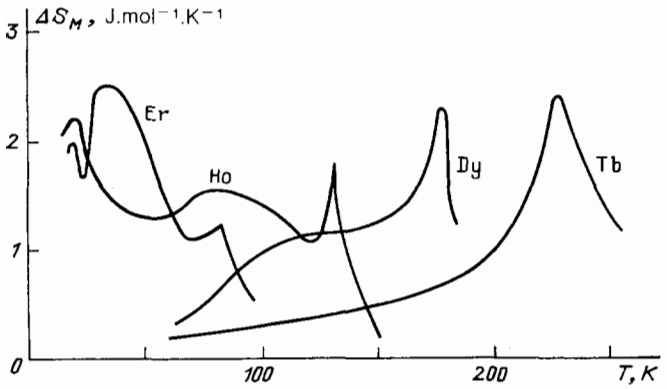

FIG. 13. Temperature dependences of the change in the magnetic part of the entropy ΔS_M in a field $H = 60.2$ kOe applied to Er, Ho, Dy, and Tb.

order helicoidal antiferromagnetism–fan structure phase transitions.

Using the data on the MCE and specific heat of heavy rare-earth metals we can calculate the temperature dependence of the change in the magnetic part of the entropy $\Delta S_M(H,T)$ on application of an external magnetic field using the following thermodynamic relationship:

$$\Delta S_M(H, T) = -\frac{\Delta T C_P(H, T)}{T}, \qquad (3.2)$$

where ΔT is the MCE. The temperature dependences of ΔS_M calculated using this expression are plotted in Fig. 13 for heavy rare-earth metals. We can see that the maximum increase in the magnetic part of the entropy ΔS_M in the field is observed near the magnetic phase transitions Θ_1 and Θ_2 (Ref. 28).

We shall now compare the change in the magnetic part of the entropy $\Delta S_M^{\Theta_2}$ at the point Θ_2 in a field $H = 60.2$ kOe with the maximum entropy S_M^{max}, which can be calculated assuming that the applied magnetic field is infinitely high and that the investigated metal is an ensemble of trivalent free ions with the total mechanical momentum governed by the quantum number J. In the statistical model of Ref. 25 the magnetic part of the entropy is due to complete disorder in the orientation of the magnetic moments in such an ensemble and it amounts to

$$S_M^{max} = R \ln(2J + 1), \qquad (3.3)$$

where R is the universal gas constant.

Table III lists the published values of S_M^{max} and $\Delta S_M^{(\Theta_2)}$ in a field $H = 60.2$ kOe given in Refs. 20 and 25 for heavy rare-earth metals. We can see that the values of S_M^{max} and $\Delta S_M^{(\Theta_2)}$ differ by about an order of magnitude. According to the theory of Ref. 37, near the point Θ_2, we have $\Delta C \propto H^{2/3}$. Hence, it follows that the maximum values of the MCE can be obtained if we use fields of the order of several hundreds of kilo-oersted. The MCE in such fields should be an order of magnitude higher than the values measured in $H \sim 60.2$ kOe, i.e., it should amount to $\Delta T \sim 10^2$ K. This conclusion agrees with the theoretical estimates for Tb obtained in Ref. 26.

We shall now consider in greater detail the change in the entropy of ytterbium in a magnetic field at temperatures corresponding to the magnetically ordered state. The temperature dependence of the MCE in a Tb single crystal (Fig. 14) and the published data on the temperature dependence of the specified heat of Tb (Ref. 27) make it possible to find the thermodynamic functions which are the entropy and specific heat in a magnetic field. The thermodynamic relationship

$$S - S_0 = \int_{T_0}^{T} \frac{C_P(H, T)}{T} dT, \qquad (3.4)$$

where S_0 is the entropy at $T = 0$ K and S is the entropy at some finite temperature, can be used to calculate the temperature dependence of the entropy $S(H,T)$ if we know the temperature dependence of the specific heat $C_P(H,T)$.

Integrating the $C_P(0,T)$ curve given for Tb in Ref. 27 with respect to temperature we can find from Eq. (3.4) the temperature dependence of the entropy of terbium. The value of S_0 at $T = 0$ can be assumed to be zero in accordance with the Nernst theorem.

Since in the course of measurements of the MCE a sample is under adiabatic conditions, the temperature dependence of the entropy $S(H,T)$ in a field $H \neq 0$ can be found by shifting the $S(0,T)$ curve, deduced from the specific heat data for $H = 0$, by an amount equal to the MCE measured at the temperature in question in a magnetic field. A magnetic field alters only the magnetic part of the entropy, since the corresponding changes in the phonon and electron contributions to the specific heat are negligible.

The thermodynamic relationship

TABLE III. Maximum values of the magnetic anisotropy in the case of total disorder of the orientation of the magnetic moments S_M^{max} and the change in the entropy $S_M^{(\Theta_2)}$ in a field $H = 60.2$ kOe at the temperature Θ_2 of heavy rare-earth metals.

	Tb	Dy	Ho	Er
$\Delta S_M^{(\Theta_2)}$, J.mol^{-1}.K^{-1}	2.4	2.3	1.8	1.2
S_M^{max}, J.mol^{-1}.K^{-1}	21.29	23.02	23.52	23.02

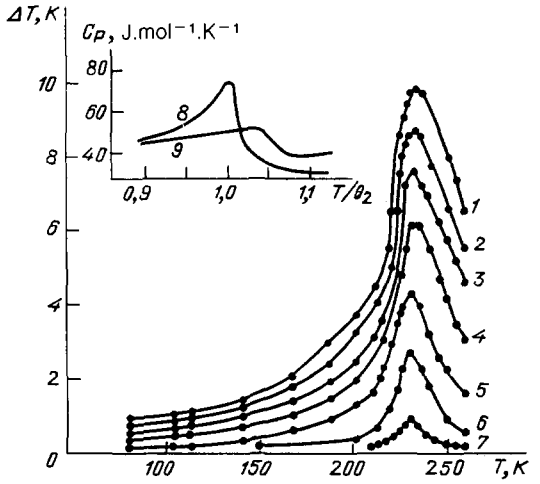

FIG. 14. Magnetocaloric effect in a Tb single crystal subjected, along the b axis, to different fields H (kOe): (1) 60.2; (2) 50.2; (3) 40.2; (4) 30.1; (5) 20.1; (6) 10; (7) 2.5. The inset shows the temperature dependences of the specific heat of a terbium single crystal in fields $H = 0$ (8) and 60.2 kOe (9).

$$C_{P,H} = T\left(\frac{\partial S}{\partial T}\right)_{P,H} \tag{3.5}$$

can be used to calculate the temperature dependence of the specific heat in a magnetic field by differentiating the $S(H,T)$ curve with respect to temperature.

The results of such calculations[20] in a field $H = 60.2$ kOe are plotted as an inset in Fig. 14 (curve 2) together with the experimentally determined[27] temperature dependence of the specific heat of terbium in $H = 0$ (curve 1). We can see that the magnetic field reduces the amplitude of the specific heat maximum and spreads it out on the temperature scale, shifting it toward higher temperatures compared with the maximum in zero field (the shift is 7.5 K in $H = 60.2$ kOe).

This effect can be explained bearing in mind that in a magnetic field a phase transition at the point Θ_2 strictly speaking disappears since the magnetic ordering exists both above and below the point Θ_2. Nevertheless, even in this case we can define a temperature $\Theta_2(H)$ at which the change in the long-range magnetic order and, consequently, in the magnetic part of the entropy occurs most rapidly when a sample is cooled. This temperature corresponds to the maximum in the dependence $C_p(H,T)$. A shift of this maximum toward higher temperatures on increase in the field shows that the field increases the temperature of a rapid change in the long-range magnetic field. It can be explained by the fact that an external field enhances the effective exchange interaction field. Therefore, an investigation of the MCE makes it possible to determine the temperature shift at which there is a rapid change in the long-range order and a change in the magnetic part of the entropy under the influence of the magnetic field.

It is interesting to determine the general relationships obeyed by the magnitude of the MCE in rare-earth metals and their alloys at magnetic phase transitions. Magnetic ordering in rare-earth metals and their alloys is governed by an indirect exchange interaction mediated by conduction electrons and dependent on the atomic constants of the rare-earth ions: the spin S and the total mechanical momentum J. The paramagnetic Curie temperature, which characterizes

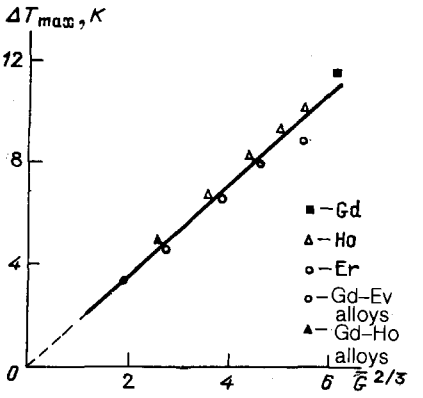

FIG. 15. Dependence of the magnetocaloric effect at the point Θ_2 in a field $H = 60.2$ kOe on the average value of the de Gennes factor $\bar{G}$.

the exchange interaction in heavy rare-earth metals, is proportional to the de Gennes factor G and the Néel temperature obeys $\Theta_2 \sim G^{2/3}$, where the factor

$$G = (g_J - 1)^2 J(J+1)$$

is the average value of the projection of the spin along the total mechanical momentum.[21]

It was established in Ref. 28 that the magnitude of the MCE of Gd–Ho and Gd–Er alloys measured at the point Θ_2 in a fixed field is proportional to $\bar{G}^{-2/3}$ (Fig. 15); here,

$$\bar{G} = \sum_i \bar{G}_i x_i,$$

where G_i is the de Gennes factor of rare-earth ion and x_i is the concentration of the rare-earth metal in an alloy.

We can thus conclude that the MCE at the point Θ_2 is governed—like other magnetic characteristics[29] including the exchange energy, the paramagnetic Curie point, the temperature Θ_2, and the difference between the exchange integrals in the ferromagnetic and antiferromagnetic states—by the average projection of the spin along the total mechanical momentum. This result is of practical interest because it allows us to forecast the magnitude of the MCE at the point Θ_2 in alloys formed by two or more heavy rare-earth metals. Variation of the ratio of these metals characterized by different values of the de Gennes factor makes it possible to prepare an alloy with the maximum MCE in a given temperature range.

We shall now consider in greater detail the MCE which appears on destruction of antiferromagnetic helicoidal structure in fields $H > H_{cr}$. This effect was investigated for Tb and Dy single crystals and $Tb_x Y_{1-x}$ alloys.[30–32] It appears because the entropies of the antiferromagnetic and ferromagnetic states are not equal. If we consider a helicoidal antiferromagnetism–ferromagnetism (HAFM–FM) transition in a field as a first-order phase transition, we find that the MCE due to a change in the entropy at this transition is

$$\Delta T_t = -\frac{T}{C_{P,H}}(S_f - S_h), \tag{3.6}$$

where $C_{P,H}$ is the specific heat; $S_f - S_h$ is the entropy jump at the transition; S_f and S_h are the entropies of the ferromagnetic and helicoidal antiferromagnetic states. We shall consider the case when the field is applied in the basal plane of

the hexagonal crystal lattice of Tb, Dy, and Tb_xY_{1-x} alloys at right-angles to the helicoidal structure axis which is parallel to the c axis. Using the difference between the thermodynamic potentials of the helicoidal and ferromagnetic phases,[33] and bearing in mind that $S = -(\partial\Phi/\partial T)_{P,H}$, we find the MCE due to the HAFM–FM transition under the influence of a magnetic field $H > H_{cr}$:

$$\Delta T_t = -\frac{T}{C_{P,H}}\left(\frac{\partial \Delta F_{exch}}{\partial T} + \frac{\partial \Delta E_{me}}{\partial T} + \frac{\partial \Delta E_A^{\delta}}{\partial T} - H_{cr}\frac{\partial \Delta I}{\partial T}\right). \quad (3.7)$$

Here, the sign of Δ denotes an abrupt change in thermodynamic quantities as a result of the HAFM–FM transition in a magnetic field. The first term in the parentheses is the result of a change in the exchange energy ΔF_{exch} between the magnetic layers at the phase transition, the second is due to a reduction in hte magnetoelastic energy ΔE_{me} in $H = H_{cr}$ mainly because of a magnetostrictive deformation along the helicoid axis (c axis), the third is related to a reduction in the magnetic anisotropy energy ΔE_A^{δ} in the basal plane, and the fourth is caused by a change in the energy of the interaction of the magnetization I with the applied magnetic field (Zeeman energy).

If we use certain thermodynamic relationships between ΔE_{me}, ΔE_A^{δ}, H_{cr}, and I established for Tb_xY_{1-x} alloys,[33] we can find from Eq. (3.7) the components of the MCE at the HAFM–FM transition.[33]

Figure 16 shows the MCE for a single crystal of the $Tb_{0.835}Y_{0.165}$ alloy in the temperature range $\Theta_1 - \Theta_2$ ($\Theta_1 = 120$ K, $\Theta_2 = 205$ K). In this range the alloy in question has a helicoidal magnetic structure.[21] We can see that in fields $H = H_{cr}(T)$ at temperatures $T > \Theta_1$ the HAFM–FM transition is accompanied by an abrupt change in the temperature of a sample. The results of calculations of the components of the MCE for this alloy are presented in Table IV, which shows that at $T = 137$ K the main contribution to ΔT_t comes from a change in the exchange energy between the layers at $H = H_{cr}$ and a change in the magnetoelastic energy, which in this case is very large because of the giant magnetostriction at the HAFM–FM transition in a magnetic field. However, as the temperature is increased, the relative value of this contribution decreases and the exchange and the magnetoelastic energy contributions then predominate. The absolute values of these contributions arise on approach to the temperature $\Theta_2 = 205$ K because of a reduction in the spontaneous magnetization of the magnetic layers in the helicoidal structure. Far from $\Theta_k = 190$ K, where $dH_{cr}/dT = 0$, the net sum of all the contributions vanishes and we have $\Delta T_t = 0$.

The MCE in Tb_xDy_{1-x} alloys[34] in the temperature range $\Theta_1 - \Theta_2$, like that in Tb_xY_{1-x} alloys, is largely due to

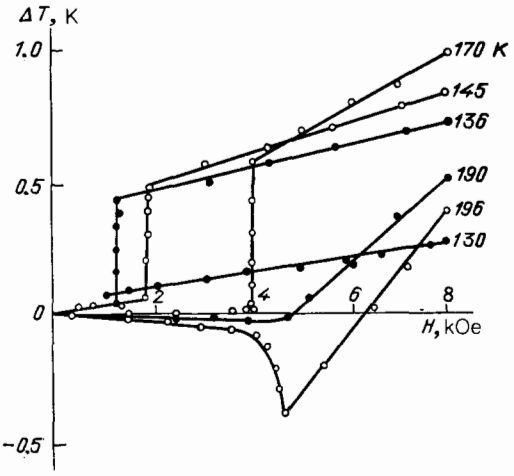

FIG. 16. Dependences of the magnetocaloric effect on the magnetic field applied to a single crystal of the $Tb_{0.835}Y_{0.165}$ alloy in the H||b configuration (ΔT is in kelvin).

the change in the magnetoelastic energy. It appears at the HAFM–FM transition because the magnetostrictive strains in the helicoidal and ferromagnetic phases differ by an amount equal to the giant magnetostriction.

Rare-earth metals and their alloys have large values of the uniaxial magnetic anisotropy constants[19] describing the anisotropy associated with rotation of the magnetic moment of a crystal relative to the hexagonal c axis. The magnetic anisotropy energy in the basal plane is considerably less. If a magnetic field is sufficiently high and exceeds considerably both H_{cr} and the effective magnetic anisotropy fields, the MCE in a magnetic field varies only slightly with the crystallographic direction. For example, when measurements are made on terbium in a field $H = 60.2$ kOe, which exceeds H_{cr} and the effective magnetic anisotropy field in the basal plane, the temperature dependences of the MCE in polycrystalline (Fig. 8) and single-crystal (Fig. 14) samples are practically identical (the value of the critical field for Tb is $H_{cr} \sim 200$ Oe).

If the applied magnetic field is comparable with the effective magnetic anisotropy field, the MCE in rare-earth metals and their alloys includes a considerable contribution from the change in the magnetic anisotropy energy due to rotation of the magnetization relative to the crystallographic axes (Kirenskiĭ effect). Moreover, the MCE observed in these metals is associated with an increase in the magnetic anisotropy constants on increase in the magnetization under the influence of the field in the paraprocess region. These effects were investigated experimentally for gadolinium[35] and Tb_xGd_{1-x} alloys.[33] Separation of the MCE due to a

TABLE IV. Components of the magnetocaloric effect at the HAFM–FM transition in a $Tb_{0.835}Y_{0.165}$ single crystal.

T, K	$\frac{T}{C_P}\frac{\partial \Delta F_{exch}}{\partial T}$, K	$\frac{T}{C_P}\frac{\partial \Delta E_{me}}{\partial T}$, K	$\frac{T}{C_P}\frac{\partial \Delta E_A^{\delta}}{\partial T}$, K	$-\frac{T}{C_P}H_{cr}\frac{\partial \Delta I}{\partial T}$, K	$(\Delta T_t)_p$, K	$(\Delta T_t)_e$, K
137	0.42	0.24	0.014	0.088	0,76	0.39
190	−1.42	0.35	0.0045	1,07	0,0045	0

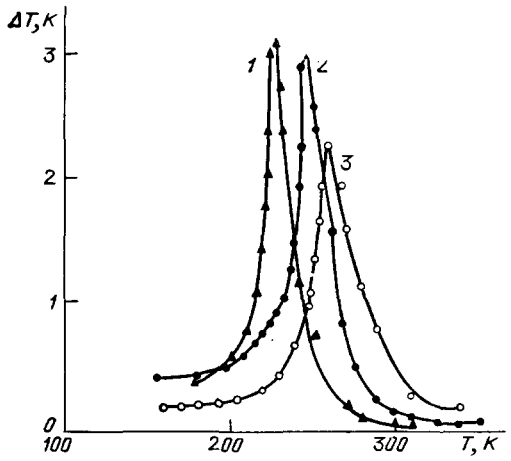

FIG. 17. Magnetocaloric effect in a field $H = 8$ kOe applied along the b axis to terbium (1) and Tb_xGd_{1-x} alloys, where $x = 0.70$ (2) and 0.20 (3).

change in the magnetic anisotropy energy ΔT_A in these crystals is made easier by the circumstance that they are ferromagnetic or antiferromagnetic with a very low value of H_{cr}, so that the MCE associated with destruction of the helicoidal structure in these materials is either absent or can be ignored.

We shall consider, for example, the temperature dependence of the MCE in Tb and Tb_xGd_{1-x} alloys along the easy magnetization axis b located in the basal plane of a hexagonal crystal (Fig. 17) and along the difficult magnetization (c) axis (Fig. 18). We can see that the MCE has a clear maximum at the Curie point T_C in a field $\mathbf{H}\|\mathbf{b}$ and the magnitude of the ΔT effect at T_C is fairly large (2–3 K) in a field 8 kOe. This maximum is due to a strong paraprocess. The Curie temperatures of the alloys determined from the MCE measurements (at the maximum) and from the magnetization (by the method of thermodynamic coefficients[37]) are in good agreement.

The temperature dependences of the MCE in a field $\mathbf{H}\|\mathbf{c}$ (Fig. 18) differ considerably in the case when the field is in the basal plane. Near T_C when $\mathbf{H}\|\mathbf{c}$ there is also a maximum, but the $\Delta T(T)$ curve is of a different nature and the maximum extends over a wider temperature interval. Moreover, if $T < T_C$, the reduction in the MCE as a result of cooling causes a reversal of the sign of the effect from positive to negative for all the samples.

At the temperature of an MCE maximum there is also a maximum of the temperature dependence of the magnetization if the MCE and the magnetization are measured in the same field $\mathbf{H}\|\mathbf{c}$. The temperature of the MCE and magnetization maxima depends strongly on the applied field which shifts them toward lower temperatures. A thermodynamic analysis of this phenomenon[38] shows that near the Curie point the paraprocess in an anisotropic ferromagnet subjected to a field $\mathbf{H}\|\mathbf{c}$ is complex. It is accompanied not only by an increase in the magnetic moment of a crystal because the field overcomes the disorienting effect of thermal motion, but also by tilting of the magnetic moment of the crystal out of the basal plane toward the c axis under the influence of the field $\mathbf{H}\|\mathbf{c}$.

A change in the sign of the MCE which occurs in this case can be explained by a change in the mechanisms resulting in the evolution and absorption of heat. Near T_C in the paramagnetic region (in a "high-symmetry" phase when $I_\parallel \neq 0$ and $I_\perp = 0$), the application of a field results in heat evolution because of an increase in the degree of magnetic order and because of a reduction in the entropy of the magnetic subsystem, which in turn increases the crystal lattice entropy as a result of adiabatic magnetization. At temperatures below the Curie point (in the "low-symmetry" phase when $I_\parallel \neq 0$ and $I_\perp \neq 0$) the dominant effect is that of the work done by the external magnetic field against the magnetic anisotropy forces. If we confine ourselves to just the main terms of the expansion of the magnetic anisotropy energy of a hexagonal crystal, we can calculate this effect at temperatures $T \ll T_C$ using an expression similar to Eq. (1.2):

$$\Delta T_A = \frac{T}{C_{P,H}}\left(\frac{\partial K_1}{\partial T}\right)_{P,H}(\sin^2\vartheta_k - \sin^2\vartheta_0), \qquad (3.8)$$

where K_1 is the first magnetic anisotropy constant; ϑ_k and ϑ_0 are the angles between the direction of the magnetization and the c axis after the application of a field H and in the absence of the field, respectively.

Since the easy magnetization axis of Tb_xGd_{1-x} alloys lies along the b axis, where $\vartheta = 90°$, $\Theta_k < \Theta_0$, $\partial K_1/\partial T > 0$, and $K_1 < 0$, it follows from Eq. (3.8) that the MCE associated with reversible rotation of the magnetization is negative (Fig. 18). Cooling makes this MCE predominant when the magnetization is along the c axis. This mechanism can account for the angular dependence of the MCE when a sample of a ferromagnetic crystal of the $Tb_{0.39}Gd_{0.61}$ alloy is rotated

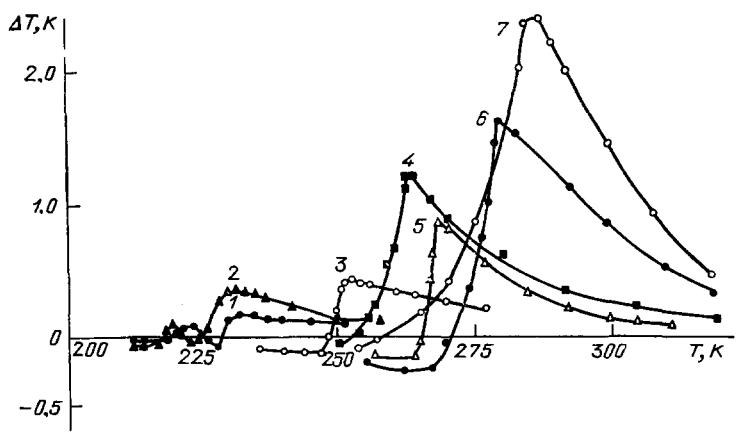

FIG. 18. Magnetocaloric effect in Tb_xGd_{1-x} alloys in a field $H = 12$ kOe applied along the c axis. Terbium content; $x =$ 1 (1) 1; (2) 0.94; (3) 0.70; (4) 0.39; (5) 0.39; (6) 0.20; (7) 0.09.

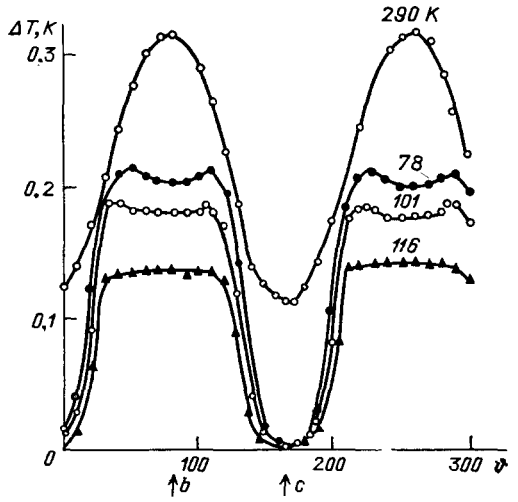

FIG. 19. Dependences of the magnetocaloric effect in $Tb_{0.39}Gd_{0.61}$ on the direction of the applied field ($H = 8.2$ kOe) in the (b,c) plane.

in a field in the (b,c) plane which includes the directions of easy and difficult magnetizations[36] (Fig. 19). We can see that in the paramagnetic region at $T = 290$ K the MCE of this alloy has a relatively simple angular dependence (the Curie point of the alloy is $T_C = 265$ K). In the case of Tb and Tb_xGd_{1-x} alloys with $x > 0.4$ the same angular dependence is observed also at lower temperatures. However, in alloys with high gadolinium concentrations (characterized by $x < 0.4$) the dependence $\Delta T(\Theta)$ becomes more complex. For example, in the case of the $Tb_{0.39}Gd_{0.61}$ alloy at temperatures from 78 to 101 K the $\Delta T(\Theta)$ curve does not have just one maximum along the c axis, but two maxima located symmetrically relative to the c axis.[36] We can explain these results on the assumption that the polar diagram representing the total energy (i.e., the anisotropy energy and the energy of the interaction of the magnetic moment of a sample with the applied field) exhibits low-temperature extrema which are additional to those along the crystallographic axes b and c. The positive sign of the MCE in $\mathbf{H}\|\mathbf{b}$ is due to the paraprocess.

Rotation of a ferromagnetic single crystal of a rare-earth alloy about the c axis in a field applied in the basal plane should give rise to the MCE associated with the change in the magnetic anisotropy energy in the basal plane. A polar diagram of the MCE observed on rotation of the magnetization in the basal plane of a single crystal of the $Tb_{0.78}Gd_{0.22}$ alloy was reported in Ref. 39 and an estimate was obtained of the anisotropic contribution ΔT_A to the MCE. In this case the magnetic anisotropy energy in the basal plane can be described by $F_A = K_6^6 \cos 6\varphi$, where φ is the angle measured from the a axis in the basal plane. At temperatures $T < T_C$ the corresponding contribution to the entropy is $S(H) = -(\partial F_A/\partial T)_H$. In the adiabatic magnetization case the change in the lattice entropy is opposite in sign to the change in the entropy of the magnetic system. Therefore, the anisotropic contribution to the MCE on rotation of the magnetization in the basal plane from the φ_0 to the angle φ_k, at which the field H is applied, is

$$\Delta T_A = \frac{T}{C_{P,H}} \left(\frac{\partial K_6^6}{\partial T} \right)_{P,H} (\cos 6\varphi_k - \cos 6\varphi_0). \qquad (3.9)$$

It follows from Eq. (3.9) that if $\varphi_0 = \pi/2$ (when the easy magnetization axis is parallel to the b axis) and $\varphi_k = 0$ ($\mathbf{H}\|\mathbf{a}$) (when the field is assumed to be higher than the saturation value), the MCE is given by

$$(\Delta T_A)_{H\|a} = \frac{2T}{C_{P,H}} \frac{\partial K_6^6}{\partial T}, \qquad (3.10)$$

and in $\mathbf{H}\|\mathbf{b}$ we have $(\Delta T_A)_{H\|b} = 0$. The angular dependence of ΔT_A predicted by Eq. (3.10) was confirmed experimentally in Ref. 39.

4. POTENTIAL TECHNICAL APPLICATIONS

New refrigerators based on utilization of the magnetocaloric effects have been proposed recently.[41–48] It is suggested that refrigerants should be rare-earth magnetic materials exhibiting a large MCE and a change in the magnetic part of the anisotropy in the temperature intervals appropriate to such refrigerators.[53,54,61]

The operating principle of a magnetic refrigerator is as follows (Fig. 20). A solid refrigerant is a magnetic material which is moved cyclically between a heat receiver and a source of heat (the body to be cooled). In a strong magnetic field the refrigerant becomes isothermally magnetized and the heat evolved in it (because of the MCE) is transmitted to the receiver. In the zone where there is no magnetic field the refrigerant becomes demagnetized so that its temperature falls and it receives heat from the source, i.e., from the body to be cooled. After an equilibrium has been re-established, the cycle is repeated. We thus have a magnetic heat pump which moves heat from the body being cooled.

This cooling method has been used for a long time in the laboratory to establish ultralow temperatures by demagnetization. It is suitable for cooling small samples from 1 to 10^{-2} K (Ref. 49). The idea was put forward by Debye[50] and Giauque.[51] The most effective refrigerant for this purpose is currently a rare-earth paramagnetic compound in the form of cerium magnesium nitrate $Ce_2Mg_3(NO_3)_{12} \cdot 24H_2O$ (Ref. 49). In view of the weak interaction of the magnetic moments of the Ce ions and the negligible influence of the crystal field on these ions, the magnetic entropy S_M of this substance varies within wide limits in a magnetic field and this is a necessary condition for the attainment of ultralow temperatures.

Optimistic forecasts on the use of other rare-earth paramagnetic compounds in magnetic refrigerators operating between 15 and 1 K were made in Refs. 42, 46, and 48. For example, it is shown in Ref. 46 that the compound

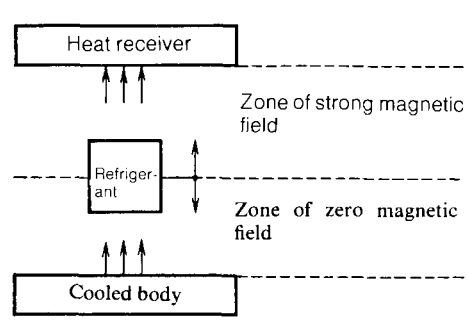

FIG. 20. Operating principle of a magnetic refrigerator.

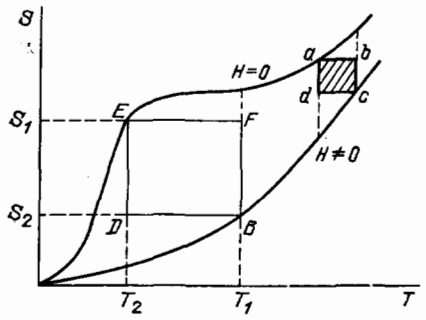

FIG. 21. Schematic temperature dependences of the entropy of rare-earth paramagnets in a magnetic field. The index *1* refers to $H = 0$ and the index *2* to $H \neq 0$. The *EFBD* and *abcd* curves represent Carnot cycles.

$Gd_2(SO_4)_3 \cdot 8H_2O$ is suitable for cooling from 4.2 K to 1.8 K, whereas in Refs. 42 and 63 it is suggested that $Gd_3Ga_5O_{12}$ gallium garnet is suitable for cooling from 16 to 4.2 K; $Dy_3Al_5O_{12}$ aluminium garnet is proposed for the same use in Refs. 48 and 63.

All these refrigerators operate on the basis of the Carnot cycle. This cycle is shown in Fig. 21 using the coordinates of the entropy and temperature. It consists of two isotherms *FB* and *DE*, and two adiabats *BD* and *EF*. The application of a field H magnetizes the refrigerant adiabatically (*EF*) and this results in the evolution of heat in the refrigerant so that its temperature rises from T_2 to T_1. The refrigerant then follows the isotherm *FB* and the heat produced by the MCE is transferred to a receiver (Fig. 20). When the point *B* is reached, the field H decreases and follows the *BD* adiabat. The refrigerant then cools by an amount $\Delta T = T_1 - T_2$. When the field is reduced to $H = 0$ the refrigerant removes heat from the body to be cooled in the isothermal section *DE*.

The result is removal of a heat $\Delta Q = T_2(S_2 - S_1)$ from the body being cooled and its transfer to the receiver. This heat transfer process occurs at the expense of the work done by an external magnetic field amounting to $(T_1 - T_2)(S_1 - S_2) = \Delta T \Delta S_M$. The magnetic cooling effect not only depends on the magnitude of the magnetocaloric effect ΔT, but also on whether S_M changes strongly on application of the field H, i.e., it depends on ΔS_M. At temperatures below 15 K such a large change is exhibited by all the rare-earth paramagnetic compounds mentioned in the preceding paragraphs. However, at temperatures $T > 15$ K, an increase in the lattice component of the entropy S_{latt} makes the Carnot cycle ineffective in magnetic refrigerators containing a paramagnetic refrigerant. In this case the Carnot cycle plotted in the entropy–temperature diagram (Fig. 21) has only a small area (*abcd*), i.e., only a small amount of heat is removed from the body being cooled in one cycle.

At higher temperatures it is more effective to use magnetically ordered substances in which a magnetic cooling effect is due to a large MCE and a large change in S_M under the influence of the field H in the range of temperatures where a magnetic ordering exists.

A magnetic refrigerator utilizing gadolinium is considered in detail in Ref. 41. Since Gd is characterized by the Curie temperature $T_C = 293$ K, this refrigerator can operate at room temperature. Figure 22 shows the operating principle of this refrigerator. A column C containing a recoverable heat-transfer liquid is set in reciprocal motion and use is made of the Stirling thermodynamic cycle in which the refrigerant interacts, in a static magnetic field,[41] with the heat-transfer liquid. Figures 22a and 22b show the first and second stages of the operation of the refrigerant: a magnetic field is applied at the moment when the refrigerant is at the top of the column (isothermal magnetization) and the column moves upward in a static field. Isothermal demagnetization (Fig. 22c) and downward motion of the column in the absence of a magnetic field (Fig. 22d) represent the subsequent stages. It was reported in Ref. 41 that a considerable cooling effect was achieved in the recoverable liquid in a magnetic refrigerator based on this principle: after 50 cycles in a field of 70 kOe the temperature in the lower part of the column was $T_{cool} = -1$ °C and in the upper part of the column it was $T_{hot} = 46$ °C.

A rotating magnetic refrigerator was proposed in Ref. 42: a suitable control of the flow of a heat carrier makes it possible to realize a regenerative or a nonregenerative cycle. The refrigerant in such a rotating refrigerator is in the form of a wheel (Fig. 23). Rotation of the wheel causes the refrigerant to pass through a zone of a high magnetic field. The wheel contains a porous gadolinium metal through which

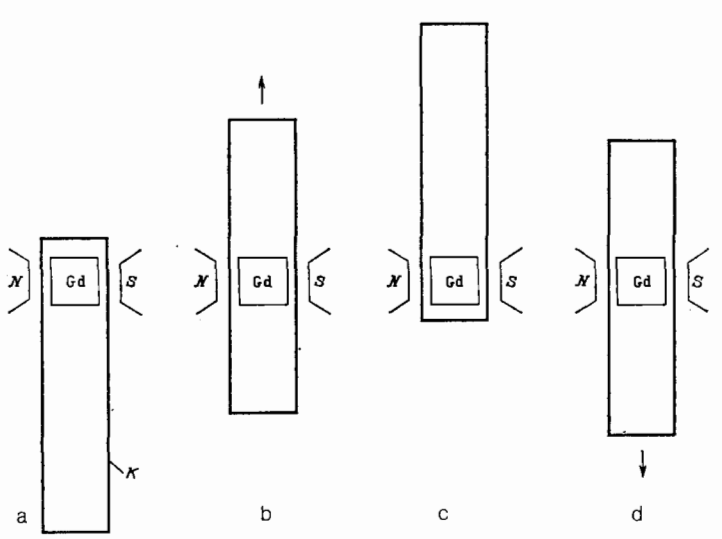

FIG. 22. Reciprocating magnetic refrigerator operating on the basis of the Stirling cycle: (a) isothermal magnetization; (b) recovery in a fixed field; (c) isothermal demagnetization; (d) recovery in zero field.

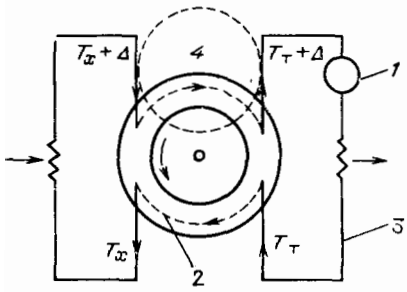

FIG. 23. Magnetic refrigerator with a wheel: (1) pump; (2) porous wheel made of the refrigerant (gadolinium); (3) heat carrier; (4) zone of action of the magnetic field.

this liquid metal is circulated by pumps in two ("cold" and "warm") loops. The cold loop removes heat and transfers it to the refrigerant, which is then exposed to the magnetic field. The heat of magnetization is removed by the warm loop, this is followed by adiabatic demagnetization, etc.

Cooling in other ranges below room temperature can be achieved utilizing the MCE near low-temperature magnetic phase transitions. As demonstrated in Secs. 2 and 3 of the present review, such transitions occur in Gd iron garnet at liquid nitrogen temperatures (low-temperature point T_{lt}) and at ferromagnetism—helicoidal antiferromagnetism transitions (point Θ_l) in rare-earth metals and alloys. Near these points such substances exhibit a large MCE and the magnetic anisotropy changes within wide limits on application of a field H.

Optimistic forecasts on the use of rare-earth intermetallic compounds as refrigerants in magnetic refrigerators have been made recently.[59,60] The system of compounds RNi_2 can be used, for example, at temperatures $T > 35$ K (Ref. 60). The results of an investigation of the specific heat and magnetization of RNi_2 compounds were used in Ref. 60 to calculate the total entropy and the change in the magnetic part of the entropy in a field. Calculations showed that these compounds can be used in certain magnetic refrigerators. Major changes in the magnetic entropy are exhibited also by RAl_2 compounds.[59] These compounds (alloys) are suitable for use at temperature above 20 K.

The advantages of such magnetic refrigerators, compared with the gas or liquid refrigerators used widely at present, are thermodynamic efficiency, compact size, wide range of working temperatures, and operational reliability. They can be used in electronics, in space research, and in other branches of technology. Operation of magnetic refrigerators requires the use of strong magnetic fields. The interest in such refrigerators has been rekindled by the progress made in the construction of miniature sources of very strong magnetic fields such as permanent magnets made of rare-earth alloys (for example, Sm–Co or Nd–Fe–B) and because of the likelihood of construction of solenoids from materials exhibiting high-temperature superconductivity.

[11]Reversal of the sign of the MCE at the magnetic compensation point of $NiCrFeO_4$ spinel was reported somewhat earlier.[6]

[1]P. Weiss and A. Piccard, C. R. Acad. Sci. **166**, 352 (1918).
[2]L. V. Kirenskiĭ, Author's Abstract of Thesis for Candidate's Degree (in Russian), Moscow State University (1939).
[3]N. S. Akulov and L. V. Kirenskiĭ, J. Phys. USSR **3**, No. 3, 31 (1940).
[4]K. P. Belov, E. V. Talalaeva, L. A. Chernikova, and V. I. Ivanovskiĭ, Pis'ma Zh. Eksp. Teor. Fiz. **7**, 423 (1968) [JETP Lett. **7**, 331 (1968)].
[5]E. V. Talalaeva, L. A. Chernikova, and V. I. Ivanovskiĭ, Vestn. Mosk. Univ. Fiz. Astron. **10**, No. 6, 113 (1969).
[6]V. I. Nikolaev, I. A. Dubovtsev, G. G. Ugodnikov, and S. S. Yakimov, Izv. Akad. Nauk SSSR Ser. Fiz. **30**, 949 (1966) [Bull. Acad. Sci. USSR **30**, 991 (1966)].
[7]K. P. Belov, Helv. Phys. Acta **41**, 679 (1968).
[8]K. P. Belov, and S. A. Nikitin, Zh. Eksp. Teor. Fiz. **58**, 937 (1970) [Sov. Phys. JETP **31**, 505 (1970)].
[9]K. P. Belov and S. A. Nikitin, Izv. Akad. Nauk SSSR Ser. Fiz. **34**, 957 (1970) [Bull. Acad. Sci. USSR **34**, 850 (1970)].
[10]K. P. Belov, Zh. Eksp. Teor. Fiz. **41**, 692 (1961) [Sov. Phys. JETP **14**, 499 (1962)].
[11]K. P. Belov, Izv. Akad. Nauk SSSR Ser. Fiz. **25**, 1320 (1961) [Bull. Acad. Sci. USSR **25**, 1332 (1961)].
[12]K. P. Belov, E. V. Talalaeva, L. A. Chernikova, T. V. Kudryavtseva, and V. I. Ivanovskiĭ, Zh. Eksp. Teor. Fiz. **62**, 2183 (1972) [Sov. Phys. JETP **35**, 1141 (1972)].
[13]K. P. Belov, E. V. Talalaeva, L. A. Chernikova, T. V. Kudryavtseva, and V. I. Ivanovskiĭ, Pis'ma Zh. Eksp. Teor. Fiz. **9**, 671 (1969) [JETP Lett. **9**, 416 (1969)].
[14]A. E. Clark, Phys. Rev. Lett. **23**, 307 (1969).
[15]K. P. Belov, S. A. Nikitin, E. V. Talalaeva, *et al.*, Zh. Eksp. Teor. Fiz. **61**, 1101 (1971) [Sov. Phys. JETP **34**, 588 (1972)].
[16]K. P. Belov, M. A. Belyanchikova, R. Z. Levitin, and S. A. Nikitin, *Rare-Earth Ferromagnets and Antiferromagnets* [in Russian], Nauka, M. (1965).
[17]S. A. Nikitin, E. V. Talalaeva, L. A. Chernikova, and A. S. Andreenko, Zh. Eksp. Teor. Fiz. **65**, 2058 (1973) [Sov. Phys. JETP **38**, 1028 (1974)].
[18]S. A. Nikitin, E. V. Talalaeva, L. A. Chernikova, and A. S. Andreenko, Fiz. Met. Metalloved. **40**, 967 (1975). [Phys. Met. Metallogr. (USSR) **40** (5), 55 (1975)].
[19]K. P. Belov, *Rare-Earth Magnetic Materials and Their Applications* [in Russian], Nauka, M. (1980).
[20]S. A. Nikitin, A. S. Andreenko, A. M. Tishin, A. M. Arkharov, and A. A. Zherdev, Fiz. Met. Metalloved. **60**, 689 (1985). [Phys. Met. Metallogr. (USSR) **60**(4), 56 (1985).
[21]K. N. R. Taylor and M. I. Darby, *Physics of Rare-Earth Solids*, Chapman and Hall, London, 1972, [Russ. Transl., Mir. M., 1974].
[22]W. Hirschler and W. Rocker, Z. Angew. Phys. **21**, 368 (1966).
[23]S. A. Nikitin and A. M. Tishin, Fiz. Tverd. Tela (Leningrad) **29**, 2812 (1987) [Sov. Phys. Solid State **29**, 1615 (1987)].
[24]R. Herz and H. Kronmüller, J. Magn. Magn. Mater. **9**, 273 (1978).
[25]L. D. Landau and E. M. Lifshitz, Statistical Physics 2nd ed., Pergamon Press, Oxford, 1969. [Russ. original, Nauka, M., 1964].
[26]V. V. Druzhinin, V. M. Mel'nikov, and V. V. Shkarubskiĭ, Fiz. Tverd. Tela (Leningrad) **21**, 1750 (1979) [Sov. Phys. Solid State **21**, 1002 (1979)].
[27]L. D. Jennings, R. M. Stanton, and F. H. Spedding, J. Chem. Phys. **27**, 909 (1957).
[28]S. A. Nikitin, A. S. Andreenko, A. M. Tishin, *et al.*, Fiz. Met. Metalloved. **59**, 327 (1985). [Phys. Met. Metallogr. (USSR) **59**(2), 104 (1985).
[29]S. A. Nikitin, *Author's Abstract of Doctoral Thesis* [in Russian], Moscow State University (1982).
[30]S. A. Nikitin, A. S. Andreenko, and V. A. Pronin, Fiz. Tverd. Tela (Leningrad) **21**, 2808 (1979) [Sov. Phys. Solid State **21**, 1616 (1979)].
[31]S. A. Nikitin, A. S. Andreenko, G. E. Chuprikov, and V. P. Posyado, Zh. Eksp. Teor. Fiz. **73**, 228 (1977) [Sov. Phys. JETP **46**, 118 (1977)].
[32]S. A. Nikitin and A. S. Andreenko, Fiz. Met. Metalloved. **52**, 67 (1981). [Phys. Met. Metallogr. (USSR) **52**(1), 55 (1981)].
[33]S. A. Nikitin, Zh. Eksp. Teor. Fiz. **86**, 1734 (1984) [Sov. Phys. JETP **59**, 1010 (1984)].
[34]S. A. Nikitin, T. I. Ivanova, P. I. Leont'ev, and E. V. Talalaeva, Vestn. Mosk. Univ. Fiz. Astron. **41**, No. 3, 52 (1986).
[35]S. A. Nikitin, E. V. Talalaeva, L. A. Chernikova, *et al.*, Zh. Eksp. Teor. Fiz. **74**, 205 (1978) [Sov. Phys. JETP **47**, 105 (1978)].
[36]S. A. Nikitin, A. S. Andreenko, and G. E. Chuprikov, Vesn. Mosk. Univ. Fiz. Astron. **36**, No. 1, 64 (1981).
[37]K. P. Belov, Magnetic Transitions, Consultants Bureau, N.Y., 1961 [Russian original, Fizmatgiz, M., 1959].
[38]S. A. Nikitin, A. S. Andreenko, A. K. Zvezdin, and A. F. Popkov, Izv. Akad. Nau, SSSR Ser. Fiz. **44**, 1343 (1980) [Bull. Acad. Sci. USSR **44**, No. 7, 14 (1980)].
[39]E. V. Talalaeva, L. A. Chernikova, S. A. Nikitin, *et al.*, Fiz. Met. Metalloved. **54**, 495 (1982). [Phys. Met. Metallogr. (USSR) **54**(3), 69 (1982)].
[40]K. P. Belov, *Elastic, Thermal, and Electrical Effects in Ferromagnets* [in Russian], Nauka, M., 1957.
[41]G. V. Brown, J. Appl. Phys. **47**, 3673 (1976).
[42]W. A. Steyert, J. Appl. Phys. **49**, 1216 (1978).

[43]V. M. Brodyanskiĭ, Nizkotemp. Protsessy Kriogen. Sist. No. 427, 34 (1979).
[44]A. M. Arkharov, N. B. Brandt, and A. A. Zherdev, Kholod. Tekh. No. 8, 13 (1980).
[45]T. Hashimoto, T. Numasawa, M. Shino, and T. Okada, Cryogenics **21**, 647 (1981).
[46]C. Delpuech, R. Beranger, G. Bon Mardion, G. Claudet, and A. A. Locaze, Cryogenics **21**, 579 (1981).
[47]A. M. Arkharov, A. A. Zherdev, S. A. Nikitin, and A. S. Andreenko, Deposited Paper No. 216–84 [in Russian], VINITI, Moscow (1983).
[48]H. Oesterreicher and F. T. Parker, J. Appl. Phys. **55**, 4334 (1984).
[49]B. I. Verkin (ed.), *Methods for Attainment and Measurement of Low and Ultralow Temperatures* [in Russian], Naukova Dumka, Kiev, 1987.
[50]P. Debye, Ann. Phys. (Leipzig) **81**, 1154 (1926).
[51]W. F. Giauque, J. Am. Chem. Soc. **49**, 1864 (1927).
[52]V. I. Ivanovskiĭ and L. A. Chernikova, *Physics of Magnetic Phenomena* [in Russian], Mir, M., 1974.
[53]S. A. Nikitin and A. M. Tishin, Deposited Paper No. 1136-V88 [in Russian], VINITI, Moscow (1988).
[54]M. E. Wood and W. H. Potter, Cryogenics **25**, 667 (1985).
[55]A. Herpin and P. Meriel, C. R. Acad. Sci. **245**, 650 (1957).
[56]E. Bertaut, F. Forrat, A. Herpin, and P. Meriel, C. R. Acad. Sci. **243**, 898 (1956).
[57]E. Prince, Acta Crystallogr. **10**, 787 (1957).
[58]V. G. Bessergenev, V. V. Gogava, A. G. Mandzhavidze, *et al.*, Pis'ma Zh. Eksp. Teor. Fiz. **47**, 92 (1988) [JETP Lett. **47**, 110 (1988)].
[59]T. Hashimoto, K. Matsumoto, T. Kurihara, *et al.*, Adv. Cryog. Eng. Mater. **32**, 279 (1986).
[60]T. Tomokiyo, H. Yayama, H. Wakabayashi, *et al.*, Adv. Cryog. Eng. Mater. **32**, 295 (1986).
[61]S. A. Nikitin and A. M. Tishin, Pis'ma Zh. Tekh. Fiz. **14**, 735 (1988) [Sov. Tech. Phys. Lett. **14**, 327 (1988)].
[62]A. S. Andreenko, Author's Abstract of Thesis for Candidate's Degree [in Russian], Moscow State University (1978).
[63]T. Hashimoto, T. Numasawa, Y. Watanabe, *et al.*, *Proc. Ninth Intern. Cryogenic Engineering Conf.* (ICEC-9), Kobe, Japan, 1982, Butterworths, Guildford, England (1982), p. 26.
[64]T. Hashimoto, T. Numasawa, and M. Shino, Physica B (Utrecht) **108**, 1107 (1981).
[65]A. M. Tishin, *Author's Abstract of Thesis for Candidate's Degree* [in Russian], Moscow State University, 1988.

Translated by A. Tybulewicz